Differential remodelling of peroxisome function underpins the environmental and metabolic adaptability of diplonemids and kinetoplastids

Short title: Gluconeogenic compartment in diplonemids

Jorge Morales[1,9], Muneaki Hashimoto[1,11], Tom A. Williams[2,3,11], Hiroko Hirawake-Mogi[1,11], Takashi Makiuchi[1,10], Akiko Tsubouchi[1], Naoko Kaga[4], Hikari Taka[4], Tsutomu Fujimura[4], Masato Koike[5], Toshihiro Mita[1], Frédéric Bringaud[6], Juan L. Concepción[7], Tetsuo Hashimoto[8], T. Martin Embley[2] and Takeshi Nara[1]*

[1]Department of Molecular and Cellular Parasitology, [4]Division of Proteomics and Biomolecular Science, and [5]Department of Cellular and Molecular Neuropathology, Juntendo University Graduate School of Medicine, 2-1-1 Hongo, Bunkyo-ku, Tokyo 113-8421, Japan

[2]Institute for Cell and Molecular Biosciences, Catherine Cookson Building, Framlington Place, Newcastle University, Newcastle upon Tyne NE2 4HH, UK

[3]School of Earth Sciences, University of Bristol, Bristol BS8 1TG, UK.

[6]Centre de Résonance Magnétique des Systèmes Biologiques (RMSB) UMR 5536 CNRS Université de Bordeaux, France

[7]Laboratorio de Enzimología de Parásitos, Facultad de Ciencias, Universidad de Los Andes, Mérida 5101, Venezuela

[8]Graduate School of Life and Environmental Sciences, University of Tsukuba, 1-1-1 Tennoudai, Tsukuba, Ibaraki 305-8572, Japan

*Correspondence: tnara@juntendo.ac.jp

Footnote

[9]Present address: Emmy Noether-Gruppe "Microbial Symbiosis and Organelle Evolution", Heinrich-Heine-Universität Düsseldorf, Universitätsstr. 1, 40225 Düsseldorf, Germany

[10]Present address: Department of Infectious Diseases, Tokai University School of Medicine, Isehara, Kanagawa 259-1193, Japan

[11]These authors contributed equally to this work.

Abstract

The remodelling of organelle function is increasingly appreciated as a central driver of eukaryotic biodiversity and evolution. Kinetoplastids including *Trypanosoma* and *Leishmania* have evolved specialised peroxisomes, called glycosomes. Glycosomes uniquely contain a glycolytic pathway as well as other enzymes, which underpin the physiological flexibility of these major human pathogens. The sister group of kinetoplastids are the diplonemids, which are among the most abundant eukaryotes in marine plankton. Here we demonstrate the compartmentalisation of gluconeogenesis, or glycolysis in reverse, in the peroxisomes of the free-living marine diplonemid, *Diplonema papillatum*. Our results suggest that peroxisome modification was already underway in the common ancestor of kinetoplastids and diplonemids, and raise the possibility that the central importance of gluconeogenesis to carbon metabolism in the heterotrophic free-living ancestor may have been an important selective driver. Our data indicate that peroxisome modification is not confined to the kinetoplastid lineage, but has also been a factor in the success of their free-living euglenozoan relatives.

Keywords

organelle evolution; metabolic compartmentalisation; peroxisomes; glycolysis; diplonemids; kinetoplastids

1. Introduction

Glycolysis (the Embden–Meyerhof-Parnas pathway) and gluconeogenesis are common to all domains of life and play fundamental roles in essential cellular processes. Glycolysis consists of 10 enzymatic steps and generates ATP, NADH, and intermediate metabolites for a variety of metabolic processes, while gluconeogenesis produces glucose 6-phosphate (G6P) from other carbon sources including lipids and amino acids [1]. Glycolysis takes place in the cytosol but glycolytic enzymes have also been associated with the plasma membrane of erythrocytes [2] and with mitochondria [3, 4]. In addition, enzyme isoforms with non-glycolytic roles are found to locate to other compartments [5].

Relocation of the first 7 of 10 glycolytic enzymes to microbody-like organelles, called glycosomes, was first demonstrated in the kinetoplastid parasite, *Trypanosoma brucei* [6], and subsequently in other kinetoplastids [7]. So far the kinetoplastids, which comprise bodonids and trypanosomatids, are the only organism known to sequester a successive glycolytic cascade into organelles. These enzymes are targeted to glycosomes by a peroxisomal targeting signal (PTS), implying that glycosomes originated as modified peroxisomes. Glycosomes also contain enzymes of other pathways including gluconeogenesis, the pentose phosphate pathway, energy/redox metabolism, and nucleotide synthesis [7]. Glycosomes are thus a classic example of how complex and physiologically important metabolic pathways can be relocated during evolution.

The relocation of entire metabolic pathways in eukaryotes is rarely observed, because isolation of the individual pathway enzymes by transfer from one compartment to another can abolish otherwise tightly coordinated enzymatic cascades. To overcome these difficulties, a “minor-mistargeting” mechanism has been proposed to allow for the dual location of pathways

[8]. According to this hypothesis, the imperfect targeting of PTS-tagged enzymes to peroxisomes would allow for the retention of functional glycolysis in the cytosol until the newly routed peroxisomal enzymes could reconstitute the pathway. This hypothesis provides a plausible mechanism for how functional retargeting could occur, but does not identify the physiological conditions or selective pressures that might drive the initial evolution of compartmentalisation.

The phylum Euglenozoa currently contains the euglenoids, diplonemids and kinetoplastids, with diplonemids the sister group of kinetoplastids and euglenoids the outgroup to both [9]. In euglenoids, glycolysis occurs in the cytosol but some enzymes are also located to its secondary plastid to participate in the Calvin cycle, as in plants and green algae [10, 11]. In the free-living marine diplonemid *Diplonema papillatum*, we have previously reported that fructose-1,6-biphosphate aldolase (FBPA), the 4th enzyme of glycolysis, has a type-2 PTS (PTS2) and is compartmentalized [12], suggesting that the transition to glycosomes may have already occurred in the common ancestor of diplonemids and kinetoplastids.

2. Materials and methods

(a) Organisms

Diplonema papillatum (strain ATCC® 50162) and the kinetoplastid *Trypanosoma cruzi* (Tulahuen stock), were grown axenically in ATCC® 1532 and 1029 media, respectively. ATCC 1532® medium contains 0.1% (w/v) tryptone and 1% horse serum, corresponding to 10 mM amino acid ingredients and 40-60 μM glucose, respectively. ATCC 1029® LIT medium is a rich medium that contains 6 mM glucose and 0.9% (w/v) liver infusion broth/0.5% tryptone,

equivalent to > 100 mM amino acid ingredients. All experiments were carried out using the standard medium unless otherwise stated.

(b) Draft genome sequencing o*f D. papillatum*

D. papillatum genomic DNA was extracted using standard protocols, purified on agarose gel to remove mitochondrial DNA, and used for genome sequencing. The *D. papillatum* genomic DNA was sequenced using a HiSeq 2000 apparatus (Illumina K.K., Tokyo, Japan) by Takara Bio Inc., Shiga, Japan and Eurofins Genomics K.K., Tokyo, Japan. Total reads were 21.5 Gb and the estimated genome size was 176.5 Mb. The *D. papillatum* open reading frames for genes of interest were identified using TBLASTN. We predicted PTS1 by the Prosite pattern PS00342 for the C-terminal tripeptides, [-(STAGCN)-(RKH)-(LIVMAFY)], and the PTS 1 Predictor (http://mendel.imp.ac.at/pts1/) [13]; we required a positive identification from both methods to diagnose the presence of a bona fide PTS. The presence of a PTS2 was manually inspected based on the N-terminal nonameric consensus sequence, (RK)-(LIV)-X5-(QH)-(LA) [14]. The *T. brucei* glycosomal proteins obtained by detailed proteomic analysis were used as references [15].

(c) Phylogenetics

We used the *D. papillatum* sequences as queries in BLASTP searches against the other euglenozoan genomes and a broad selection of outgroups. The *Euglena gracilis* PFK sequence was obtained from http://euglenadb.org/. Sequences were aligned with Meta-Coffee [16]. Poorly-aligning regions were masked using the “automated1” option in trimAl [17]. Phylogenies were built using the LG [18], C20, and C60 [19] in PhyloBayes. The trees inferred under the three methods were very similar, with no differences impacting on our inferences of the relationships

among the euglenozoans, and the consensus trees in figures 1, S1 to S5 and S8 to S10 were inferred using the C60 model.

(d) Indirect immunofluorescence analysis

Antisera to glycolytic enzymes were obtained as described in supplementary materials and methods. Indirect immunofluorescence analysis was performed as described [12]. Briefly, cells were fixed with 2% paraformaldehyde, probed with antisera to each glycolytic enzyme, and then treated with anti-rabbit Alexa-fluor 488-conjugate (Life Technologies), followed by counterstaining of the nucleus with Hoechst 33342 dye. Fluorescence was observed using fluorescence microscopy (Axio Imager M2, Carl Zeiss Co. Ltd., Tokyo, Japan).

(e) Glucose and amino acid consumption

D. papillatum cells of the mid-log phase were cultured in ATCC® 1532 medium supplemented with 6 mM D-glucose, while *T. cruzi* cells were cultured in LIT medium. The glucose concentration of the culture supernatant was measured using a Glucose-Oxidase assay kit (Sigma-Aldrich). Amino acid consumption by cells was evaluated by the increase of NH_4^+ in the culture supernatant using the Ammonia assay kit (Sigma-Aldrich).

(f) Metabolic labeling

Cells in the mid-log phase of growth were starved in artificial seawater (ATCC® 1405 HESNW medium) for 2 hrs and then incubated with 6 mM $^{13}C_6$ D-glucose or 6 mM $^{13}C_5$ L-glutamine (Sigma-Aldrich) in artificial seawater for 0, 4, and 8 hrs or with 30 mM $^{13}C_6$ D-glucose in ATCC® 1532 medium for 72 hrs without starvation. The detailed experimental procedures for

extraction of metabolites and analysis by CE-Q-TOFMS and LC-MS were described in the supplementary materials and methods.

3. Results

(a) Identification of peroxisome targeting signals in the glycolytic enzymes of *D. papillatum*

To investigate glycolytic compartmentalisation in diplonemids, we sequenced the genome of *D. papillatum* and identified all of the genes for glycolysis (table 1). We identified putative PTS for 2 types of hexose kinase, namely a high-affinity type hexokinase (HK) and a low-affinity type glucokinase (GLK), and for phosphoglucose isomerase (PGI) and phosphoglycerate kinase (PGK), similar to kinetoplastid homologues. We identified two homologues of phosphofructokinase (PFK), PFK1 and PFK2, in the genome assembly. PFK1 possesses a predicted PTS1 but is likely a pseudogene or a bacterial contaminant (see below). We also found a PTS for triose-phosphate isomerase (TIM), despite of the absence of an apparent PTS in the kinetoplastid TIM. By contrast, putative PTS were absent from the predicted coding sequences of PFK2, phosphoglycerate mutase (PGAM, 2,3-bisphosphoglycerate-independent type), enolase (ENO), pyruvate kinase (PK) and two isoforms of glyceraldehyde-3-phosphate dehydrogenase (GAPDH).

Phylogenetic analysis demonstrated that most of these enzymes (HK, GLK, PGI, PGK, ENO and PK) were present in the common ancestor of *D. papillatum* and kinetoplastids (figures S1, S2, and S3). The phylogeny for TIM was weakly supported and hence cannot reject the hypothesis of a single common origin for TIM (figure S1*d*). In contrast, three glycolytic enzymes

– PFK1 and PFK2, the two isoforms of GAPDH, and PGAM – appear to have separate evolutionary origins for *D. papillatum* and the kinetoplastids (figures 1, S1*e*, and S4).

The protein phylogeny for PFK revealed that *E. gracilis* and kinetoplastids are monophyletic with high posterior support (PP = 0.99), suggesting their shared evolutionary origin (clade A, figure 1). By contrast, *D. papillatum* PFK2 clusters with a PFK homologue from the haptophyte *Emiliania huxleyi* (PP = 1) and is nested within a different eukaryotic clade (Clade B, PP = 0.99), suggesting replacement of the ancestral euglenozoan PFK by lateral gene transfer. *D. papillatum* PFK1 detected in our genome assembly is likely a pseudogene or a bacterial contaminant: it does not group with other eukaryotic PFKs in the tree; the putative *pfk1* gene lacks a splice acceptor site at its 5'-untranslated region, which is essential for trans-splicing in euglenozoans; and we were unable to detect any PFK activity in the *D. papillatum* lysate (table 1). In summary, our data suggest that PTS-driven relocation of most, but not all, glycolytic enzymes had already occurred in the common ancestor of diplonemids and kinetoplastids.

We also investigated the presence of a PTS in the non-glycolytic enzymes of *D. papillatum*. Among 18 PTS-harboring enzymes specific to kinetoplastid glycosomes, only three of these enzymes were also predicted to have PTS in *D. papillatum*, which participate in gluconeogenesis and energy metabolism (tables 1 and S1). These include the gluconeogenic fructose-1,6-biphosphatase (FBPase) that catalyzes the reverse reaction to PFK, ATP-producing glycerol kinase (GK) and pyruvate phosphate dikinase (PPDK). None of the enzymes identified for the *Diplonema* pentose phosphate pathway (PPP), pyrimidine biosynthesis, or purine salvage were predicted to locate to peroxisomes. Notably, despite of the presence of PTS1, the protein phylogeny of FBPase revealed different evolutionary origins between *D. papillatum* and kinetoplastids, implying independent LGT events and convergent PTS-driven relocation of

FBPase in *D. papillatum* and kinetoplastids (table 1 and figure S5). Our data suggest that metabolic compartmentalisation originated in association with glycolysis, gluconeogenesis and energy metabolism in the common ancestor of *D. papillatum* and kinetoplastids.

(b) Localisation of PTS-harboring glycolytic enzymes in the peroxisomes of *D. papillatum*

To investigate the expression and confirm the cellular location of the *D. papillatum* glycolytic enzymes, we raised antisera to 11 glycolytic enzymes including GLK. Western blot analysis of the *D. papillatum* extracts showed the expected band for all enzymes tested, with the exception of the two homologues of PFK and HK (figure S6*a*). The absence of the signals for both PFK1 and PFK2 suggests that neither of the two PFK homologues is expressed or functional in the culture condition of *D. papillatum*, consistent with the lack of PFK activity. To confirm the absence of HK, we measured hexose kinase activity in *D. papillatum* cell extracts and found that the K_m value for glucose of the native enzyme harboring hexose kinase activity was 0.33 mM, whereas the K_m values of the recombinant HK and GLK were 0.064 and 0.66 mM, respectively. These results suggest that the native hexose kinase activity is likely attributable to GLK in *D. papillatum* under the experimental conditions.

Indirect immunofluorescence analysis (IFA) was performed to investigate the cellular location of the glycolytic enzymes expressed in *D. papillatum*. Our previous study showed that our mouse antiserum to *D. papillatum* FBPA detected a single band on western blots of the membrane-rich fraction (10,500 x *g* sediment) from the *D. papillatum* extract and also demonstrated the punctate pattern in the cell by IFA [12]. Immuno-electron microscopy using the same antiserum also detected labeling of FBPA inside single-membrane compartments with the characteristic morphology of peroxisomes (figure S6*b*). Therefore, we used FBPA as a

peroxisomal marker. The signals for GLK, PGI, TIM, and PGK co-localised with that of FBPA, indicating their shared peroxisomal location (figure 2). The signal for the anti-GAPDH1 antibody gave a patchy distribution in the cytosol but did not co-localise with FBPA, consistent with the absence of a PTS. PTS-lacking PGAM, ENO, and PK were also exclusively detected in the cytosol of *D. papillatum*, similar to their kinetoplastid PTS-lacking homologues.

(c) Preference of amino acids as carbon source in *D. papillatum*

The failure to detect PFK activity in *D. papillatum* suggests that the glycolytic enzymes together with FBPase play a replenishing role for gluconeogenesis in this organism. Notably, *D. papillatum* can grow with a trace level of glucose. The modified ATCC 1532 medium supplemented with 1% dialyzed fetal bovine serum (Thermo Fisher Scientific Inc.), which corresponds to < 2.7 μM glucose, can also support the normal growth of *D. papillatum* (data not shown). However, the growth of *D. papillatum* even in the absence of glucose does not necessarily indicate the loss of glucose uptake and glycolytic activity. Therefore, we investigated firstly the relative preference of carbon sources in *D. papillatum*. Consistent with our hypothesis, *D. papillatum* does not significantly consume glucose (6 mM), but preferentially uses amino acids (figure 3*a*, left). This is demonstrated by the significant production of ammonium in the presence of glucose during early exponential growth. By contrast, epimastigotes (an insect form) of the parasitic kinetoplastid *Trypanosoma cruzi* prefer glucose to amino acids, as previously reported [20]. In experiments with *T. cruzi* (figure 3*a*, right), the levels of glucose decreased significantly at day 3 to 6 along with exponential growth and became undetectable (< 10 μM) at day 7, while the levels of ammonium remained constantly by day 5 and then increased

significantly. Because amino acids are the major nutritional components in the diet of phagocytic heterotrophs like *D. papillatum*, this preference likely reflects nutritional adaptation.

(d) Gluconeogenesis is the central carbon metabolism in *D. papillatum*

To investigate the metabolic fate of amino acids, we performed tracer experiments using 6 mM ^{13}C-uniformly labeled ($^{13}C_5$, +5 carbons) L-glutamine, and *D. papillatum* cells which had been starved in artificial seawater for 2 hours prior to labeling. We detected specific enrichment with +5 carbon in the α-ketoglutarate fraction, indicating that glutamine is readily catabolized and incorporated into metabolites of the TCA cycle of *D. papillatum* (figures 3*b* and S7*a*). The presence of +5 and +6 carbons in the citrate fraction also indicated an active TCA cycle and the recycling of labeled oxaloacetate. The time-dependent increase of ^{13}C-labeling with +1 to +6 carbons for hexose phosphates provided evidence of active gluconeogenesis. In addition, the extensive metabolic dilution of ^{13}C-isotopologues in the hexose 6-phosphate fractions indicated the presence of an internal carbon source. Quantitative metabolomics demonstrated that *D. papillatum* contains higher amounts of free amino acids when compared to *T. cruzi*, suggesting that they may serve as a carbon reservoir (table S2). We conclude that amino acids are the preferred carbon/energy source for *D. papillatum* and that they are catabolized via the TCA cycle and can subsequently be anabolized via gluconeogenesis.

(e) The pentose phosphate pathway complements *PFK*-deficiency in the glycolytic process

Metabolic labeling using 6 mM $^{13}C_6$-D-glucose as a sole external carbon source showed enrichment with +1 to +5 carbons in the hexose phosphate fractions, indicating the occurrence of glucose catabolism in *D. papillatum* at a very low rate (figures 3*c* and S7*b*). Importantly,

sedoheptulose 7-phosphate (S7P), an intermediate metabolite of PPP, was significantly labeled with +1 to +6 carbons (figure 3*c*). Glucose uptake by *D. papillatum* was further investigated by cells incubated for 72 hrs in normal medium containing 30 mM $^{13}C_6$-glucose. Under these conditions, the levels of +6 carbon were significantly lower than that of +3 carbon in the hexose phosphate fractions (figure S7*c*). These data suggest that G6P is catabolized via the PPP to produce triose phosphates and their subsequent catabolites, which can then be recycled to form hexose phosphate species. Quantitative determination of the glycolytic metabolites also showed a relative accumulation of hexose phosphates in *D. papillatum* compared to *T. cruzi*, regardless of the nutritional conditions (table S2), suggesting the predominance of anabolism towards the production of hexose phosphates. Taken together, these data demonstrate that glycolysis does not significantly contribute to central carbon metabolism in *D. papillatum* and that gluconeogenesis from amino acids is the dominant process.

(f) Retargeting of non-glycolytic pathway enzymes to peroxisomes occurred in the common ancestor of kinetoplastids

To investigate the evolution of kinetoplastid glycosomes after the split from the diplonemid lineage, we inferred additional phylogenies for PTS-harboring enzymes specific to kinetoplastids. Both the phylogeny of adenylate kinase – which catalyzes the reversible interconversion of 2 ADP into ATP plus AMP – and of inosine 5-monophosphate dehydrogenase – a purine salvage enzyme – revealed that the glycosomal forms of these enzymes have been acquired laterally from bacteria in kinetoplastids (figures S8 and S9). Thus, kinetoplastids encode two copies of these genes: an ancestral copy shared with *D. papillatum,* and a glycosomal copy obtained by LGT. The phylogeny of a PPP enzyme, transketolase, showed monophyly of *D. papillatum* and

kinetoplastids within the eukaryotic clade, indicating that the ancestral forms of this enzyme were retargeted to the glycosomes in the lineage leading to kinetoplastids (figure S10). The phylogeny of other PTS-targeted enzymes was ambiguous, largely due to a lack of resolution commonly encountered in single-gene trees. We conclude that the transfer to the glycosomes of non-glycolytic enzymes, including those for pyrimidine biosynthesis [21], occurred on the branch leading to the kinetoplastids after their split from the diplonemid lineage (figure 4).

4. Discussion

Recent advances in our sampling of microbial eukaryotic diversity have begun to shed light on the unique biological features of diplonemids, not only as a relative of important human pathogens but also as a major protistan group in ocean plankton [22, 23]. The ecological success of diplonemids as marine plankton [23] suggests that independence from glucose accompanied by peroxisome remodelling is a viable strategy for heterotrophic life. Our draft genome sequencing of *Diplonema* provides an important source of genomic data for this group.

The phylogeny of PFK revealed that kinetoplastid and *E. gracilis* PFKs share the same evolutionary origin. Therefore, it is likely that, as well as euglenoids, a common ancestor of diplonemids and kinetoplastids utilized PFK to perform glycolysis. Whether this ancestral PFK had already relocated to peroxisomes in their common ancestor is, as yet, unclear. By contrast, *D. papillatum* PFK2 shares the same origin with a PFK homologue of the haptophyte, *E. huxleyi*. *E. huxleyi* is the most prominent marine cosmopolitan phytoplankton and often causes coccolithophore blooms [24]. It is possible that marine heterotrophs like *Diplonema* feed on

haptophytes, which may have been an evolutionary source of LGT; alternatively, both *E. huxleyi* and *D. papillatum* may have obtained these PFK genes by LGT from other members of clade B.

Our data demonstrate that the remodelling of peroxisome function already occurred in the common ancestor of diplonemids and kinetoplastids, and involved the retargeting of at least a subset of glycolytic enzymes and GK and PPDK. It is unclear whether FBPase also relocated to peroxisomes in their common ancestor, because both FBPases have different origins. Retargeting to peroxisomes of ATP-producing GK and PPDK may be related to the requirement of ATP hydrolysis in the first seven enzymatic steps of glycolysis, in terms of the maintenance of ATP homeostasis inside the peroxisomes. That is, the maintenance of the ATP levels by the action of GK, acting in the reverse direction, and PPDK in the peroxisomes might have played an important role in maintaining the efficiency of glycolysis and gluconeogenesis in these organisms.

As with enzymatic composition of the ancestral glycosomes, the primary metabolic status in the common ancestor of diplonemids and kinetoplastids is still unclear. Our metabolome data indicate that *D. papillatum* lacks a fully functional glycolytic pathway. By contrast, our phylogenetic analyses suggest that the ancestor of diplonemids and kinetoplastids likely retained glycolysis. A possible explanation is that the gluconeogenic state of *Diplonema* may not be an ancestral, but is instead a derived feature, which was accompanied by nutritional adaptations to heterotrophic life followed by the loss of expression and activity of PFK.

From a metabolic viewpoint, it seems rational that ancestral glycosomes harbored the first seven enzymes of glycolysis and the corresponding enzymes of gluconeogenesis for completion of a contiguous enzymatic cascade (figure 4). *D. papillatum* may represent an interesting case whereby nutritional adaptations leading to glucose-independent metabolism have evolved,

resulting in peroxisomes housing gluconeogenesis ("gluconeosomes"). At the same time, preservation of glycolytic activity in kinetoplastids might have potentiated adaptation to a different mode of life, parasitism. Parasitism has developed repeatedly among kinetoplastids, and this adaptability is made possible by the compartmentalisation into glycosomes of metabolic processes that have to undergo drastic and rapid changes during some transitions in the complex life cycles [25]. Hence, the sequestering of core metabolic pathways into peroxisomes, begun in the common ancestor of diplonemids and kinetoplastids, may have laid the foundations for the success of a major clade of medically and economically important parasites. Indeed, high levels of glucose (in the millimolar range) are present in the blood and body fluids of vertebrates, which can be readily utilized by hemoflagellates as carbon source.

Data accessibility. The *D. papillatum* genome was deposited in DDBJ/EMBL/GenBank under the accession LMZG00000000. *D. papillatum* sequences for relevant enzymes reported here have been deposited individually at DDBJ (accession numbers AB970479 - AB970481, AB970483 - AB970501, LC127115, LC127507). The datasets supporting this article have been uploaded as part of the supplementary material.

Competing interest. We have no competing interests.

Author contributions. T.N. designed research; J.M., M.H., T.A.W., H.H.-M., A.T., N.K., H.T., T.F., M.K., and T.N. performed research; J.M., T.A.W. and T.N. analyzed data; F.B. and J.L.C. provided materials; T.A.W., T.Ma., T.Mi., F.B., J.L.C, and T.H. helped to draft manuscript; T.A.W. and T.M.E edited the paper; and J.M. and T.N. wrote the paper.

Acknowledgements. We thank Paul Michels for critical reading and the *Euglena gracilis* nucleotide sequencing consortium (http://euglenadb.org/) for *E. gracilis* PFK sequence.

Funding. T.N. acknowledges support from grants-in-aid for scientific research (24390102 and 25670205) and from the Foundation of Strategic Research Projects in Private Universities (S1201013) from the Ministry of Education, Culture, Sport, Science, and Technology, Japan (MEXT). T.M.E. acknowledges support from the Wellcome Trust and the European Advanced Investigator Programme. T.A.W. is supported by a Royal Society University Research Fellowship.

References

1 Gruning NM, Rinnerthaler M, Bluemlein K, Mulleder M, Wamelink MM, Lehrach H, Jakobs C, Breitenbach M & Ralser M. 2011 Pyruvate kinase triggers a metabolic feedback loop that controls redox metabolism in respiring cells. *Cell Metab.* **14**, 415-427. (doi:10.1016/j.cmet.2011.06.017).

2 Campanella ME, Chu H & Low PS. 2005 Assembly and regulation of a glycolytic enzyme complex on the human erythrocyte membrane. *Proc. Natl. Acad. Sci. USA* **102**, 2402-2407. (doi:10.1073/pnas.0409741102).

3 Giegé P, Heazlewood JL, Roessner-Tunali U, Millar AH, Fernie AR, Leaver CJ & Sweetlove LJ. 2003 Enzymes of glycolysis are functionally associated with the mitochondrion in Arabidopsis cells. *Plant Cell* **15**, 2140-2151. (doi:10.1105/tpc.012500).

4 Smith DG, Gawryluk RM, Spencer DF, Pearlman RE, Siu KW & Gray MW. 2007 Exploring the mitochondrial proteome of the ciliate protozoon *Tetrahymena thermophila*: direct analysis by tandem mass spectrometry. *J. Mol. Biol.* **374**, 837-863. (doi:10.1016/j.jmb.2007.09.051).

5 Freitag J, Ast J & Bölker M. 2012 Cryptic peroxisomal targeting via alternative splicing and stop codon read-through in fungi. *Nature* **485**, 522-525. (doi:10.1038/nature11051).

6 Opperdoes FR & Borst P. 1977 Localization of nine glycolytic enzymes in a microbody-like organelle in *Trypanosoma brucei*: the glycosome. *FEBS Lett.* **80**, 360-364.

7 Gualdrón-López M, Brennand A, Hannaert V, Quiñones W, Cáceres AJ, Bringaud F, Concepción JL & Michels PA. 2012 When, how and why glycolysis became compartmentalised in the Kinetoplastea. A new look at an ancient organelle. *Int. J. Parasitol.* **42**, 1-20. (doi:10.1016/j.ijpara.2011.10.007).

8 Martin W. 2010 Evolutionary origins of metabolic compartmentalization in eukaryotes. *Philos. Trans. R. Soc. B* **365**, 847-855. (doi:10.1098/rstb.2009.0252).

9 Simpson AG & Roger AJ. 2004 Protein phylogenies robustly resolve the deep-level relationships within Euglenozoa. *Mol. Phylogenet. Evol.* **30**, 201-212. (doi:10.1016/S1055-7903(03)00177-5).

10 Hannaert V, Brinkmann H, Nowitzki U, Lee JA, Albert MA, Sensen CW, Gaasterland T, Müller M, Michels P & Martin W. 2000 Enolase from *Trypanosoma brucei*, from the amitochondriate protist *Mastigamoeba balamuthi*, and from the chloroplast and cytosol of *Euglena gracilis*: pieces in the evolutionary puzzle of the eukaryotic glycolytic pathway. *Mol. Biol. Evol.* **17**, 989-1000.

11 Plaxton WC. 1996 The organization and regulation of plant glycolysis. *Annu. Rev. Plant Physiol. Plant Mol. Biol.* **47**, 185-214. (doi:10.1146/annurev.arplant.47.1.185).

12 Makiuchi T, Annoura T, Hashimoto M, Hashimoto T, Aoki T & Nara T. 2011 Compartmentalization of a glycolytic enzyme in *Diplonema*, a non-kinetoplastid euglenozoan. *Protist* **162**, 482-489. (doi:10.1016/j.protis.2010.11.003).

13 Neuberger G, Maurer-Stroh S, Eisenhaber B, Hartig A & Eisenhaber F. 2003 Prediction of peroxisomal targeting signal 1 containing proteins from amino acid sequence. *J. Mol. Biol.* **328**, 581-592.

14 Lazarow PB. 2006 The import receptor Pex7p and the PTS2 targeting sequence. *Biochim. Biophys. Acta* **1763**, 1599-1604. (doi:10.1016/j.bbamcr.2006.08.011).

15 Güther ML, Urbaniak MD, Tavendale A, Prescott A & Ferguson MA. 2014 High-confidence glycosome proteome for procyclic form *Trypanosoma brucei* by epitope-tag organelle enrichment and SILAC proteomics. *J. Proteome. Res.* **13**, 2796-2806. (doi:10.1021/pr401209w).

16 Moretti S, Armougom F, Wallace IM, Higgins DG, Jongeneel CV & Notredame C. 2007 The M-Coffee web server: a meta-method for computing multiple sequence alignments by combining alternative alignment methods. *Nucleic. Acids. Res.* **35**, W645-648. (doi:10.1093/nar/gkm333).

17 Capella-Gutiérrez S, Silla-Martínez JM & Gabaldón T. 2009 trimAl: a tool for automated alignment trimming in large-scale phylogenetic analyses. *Bioinformatics* **25**, 1972-1973. (doi:10.1093/bioinformatics/btp348).

18 Le SQ & Gascuel O. 2008 An improved general amino acid replacement matrix. *Mol. Biol. Evol.* **25**, 1307-1320. (doi:10.1093/molbev/msn067).

19 Quang le S, Gascuel O & Lartillot N. 2008 Empirical profile mixture models for phylogenetic reconstruction. *Bioinformatics* **24**, 2317-2323. (doi:10.1093/bioinformatics/btn445).

20 Bringaud F, Riviere L & Coustou V. 2006 Energy metabolism of trypanosomatids: adaptation to available carbon sources. *Mol. Biochem. Parasitol.* **149**, 1-9. (doi:10.1016/j.molbiopara.2006.03.017).

21 Makiuchi T, Annoura T, Hashimoto T, Murata E, Aoki T & Nara T. 2008 Evolutionary analysis of synteny and gene fusion for pyrimidine biosynthetic enzymes in Euglenozoa: an extraordinary gap between kinetoplastids and diplonemids. *Protist* **159**, 459-470. (doi:10.1016/j.protis.2008.02.002).

22 Lukeš J, Flegontova O & Horák A. 2015 Diplonemids. *Curr. Biol.* **25**, R702-R704. (doi:10.1016/j.cub.2015.04.052).

23 de Vargas C, Audic S, Henry N, Decelle J, Mahe F, Logares R, Lara E, Berney C, Le Bescot N, Probert I, et al. 2015 Ocean plankton. Eukaryotic plankton diversity in the sunlit ocean. *Science* **348**, 1261605. (doi:10.1126/science.1261605).

24 Read BA, Kegel J, Klute MJ, Kuo A, Lefebvre SC, Maumus F, Mayer C, Miller J, Monier A, Salamov A, et al. 2013 Pan genome of the phytoplankton *Emiliania* underpins its global distribution. *Nature* **499**, 209-213. (doi:10.1038/nature12221).

25 Szöör B, Haanstra JR, Gualdrón-López M & Michels PA. 2014 Evolution, dynamics and specialized functions of glycosomes in metabolism and development of trypanosomatids. *Curr. Opin. Microbiol.* **22C**, 79-87. (doi:10.1016/j.mib.2014.09.006).

Table 1. Characteristics of glycolytic enzymes of *Diplonema papillatum* (Dp).

Figure Legends

Figure 1. *Diplonema papillatum* lacks an orthologue of the glycosome-targeted phosphofructokinase (PFK) gene found in other euglenozoans. A Bayesian consensus phylogeny of PFK was inferred under the C60 model in PhyloBayes. *E. gracilis* and kinetoplastid PFKs form a monophyletic group (clade A) with high posterior support (PP = 0.99). By contrast, *D. papillatum* PFK2 clusters with a PFK homologue from the haptophyte *Emiliania huxleyi* (PP = 1) and is nested within the clade "B" (PP = 0.99). Branch lengths are proportional to the expected number of substitutions.

Figure 2. Cellular localisation of glycolytic enzymes in *Diplonema papillatum* using immunofluorescence microscopy. Cells were labeled with polyclonal antisera to GLK, PGI, TIM, GAPDH, PGK, PGAM, ENO, or PK (Target, red) and with antisera to *D. papillatum* FBPA as a peroxisomal marker (FBPA, green). Images of the same cells were merged together with the labels of Hoechst 33342 (blue) to visualize the nucleus (Merge). DIC, differential interference contrast image; Merge, merged image. Scale bar = 10 μm.

Figure 3. Carbon metabolism in *Diplonema papillatum.* (*a*) Consumption of glucose and amino acids in the culture media of *D. papillatum* (left) and *Trypanosoma cruzi* epimastigotes (right). Production of ammonium, a catabolite of amino acids, denotes the consumption of amino acids. (*b* and *c*) Metabolome analysis of *D. papillatum. D. papillatum* cells were incubated in

conditioned marine water for 2 hrs and then supplemented with $^{13}C_5$-L-glutamine (*b*) or $^{13}C_6$-D-glucose (*c*) for 0, 4, and 8 hrs. The Y-axis indicates the relative abundance (%) of each isotopomer of the relevant metabolite. The X-axis represents the number of ^{13}C in the isotopomers. Data for all metabolites in these experiments are shown in figures S7*a* and S7*b*, respectively. Data points and error bars represent the mean ± s.d. of three independent experiments.

Figure 4. A proposed metabolic model and peroxisome remodelling in Euglenozoa. (*a*) Peroxisomes (Px) and mitochondria (Mt) have been present in the last eukaryotic common ancestor (LECA), with cytosolic location of glycolysis (blue arrows), gluconeogenesis (red arrows), pentose phosphate pathway (PPP), pyrimidine biosynthesis (Pyr), and purine salvage (Pur). PFK and FBPase (FBP) are critical allosteric enzymes in glycolysis and gluconeogenesis, respectively. (*b*) After the divergence of the lineage leading to Euglenoids, the peroxisomes of the common ancestor of diplonemids and kinetoplastids were remodelled through the sequestration of a subset of glycolytic enzymes, possibly FBPase, and others (boxed in yellow). In these remodelled compartments, both glycolysis and gluconeogenesis were functional. (*c*) The ancestral diplonemids or *Diplonema* lost glycolysis accompanied by the loss of PFK activity as suggested in our analysis. (*d*) The ancestral kinetoplastid further sequestered into peroxisomes a part of enzymes for PPP, Pyr, Pur, and others such as PEPCK and NADH-fumarate reductase (boxed in blue).

Table 1. Characteristics of glycolytic enzymes of *Diplonema papillatum*.

Enzyme	PTS		Monophyly*	Activity†
	D. papillatum	***T. cruzi***		
1. HK	PTS2	PTS2	Yes (0.85)	0.92‡
1. GLK	PTS1	PTS1	Yes (0.96)	
2. PGI	PTS1	PTS1	Yes (0.93)	39.1
3. PFK	PTS1/ND	PTS1	No (0.99)	ND
3. FBPase (gluconeogenic)	PTS1	PTS1	No (1.00)	4.7
4. FBPA	PTS2	PTS2	Yes (1.00)§	14.2
5. TIM	PTS1	ND	Unresolved	123.2
6. GAPDH	ND	PTS1/ND	No (0.90)	48.5
7. PGK	PTS1	PTS1/ND	Yes (0.81)	103.7
8. PGAM	ND	ND	No (1.00)	2,100
9. ENO	ND	ND	Yes (0.99)	3.7
10. PK	ND	ND	Yes (0.98)	15.1

*Monophyly of *D. papillatum* and kinetoplastids with posterior probability in parenthesis based on the relevant protein phylogeny (figures 1 and supplementary figures).

†nmol/min/mg protein of the *D. papillatum* cell extract (see also supplemental material).

‡The activities of HK (high-affinity type) and GLK (low-affinity type) are indistinguishable.

§Ref. 12.

ND; not detected.

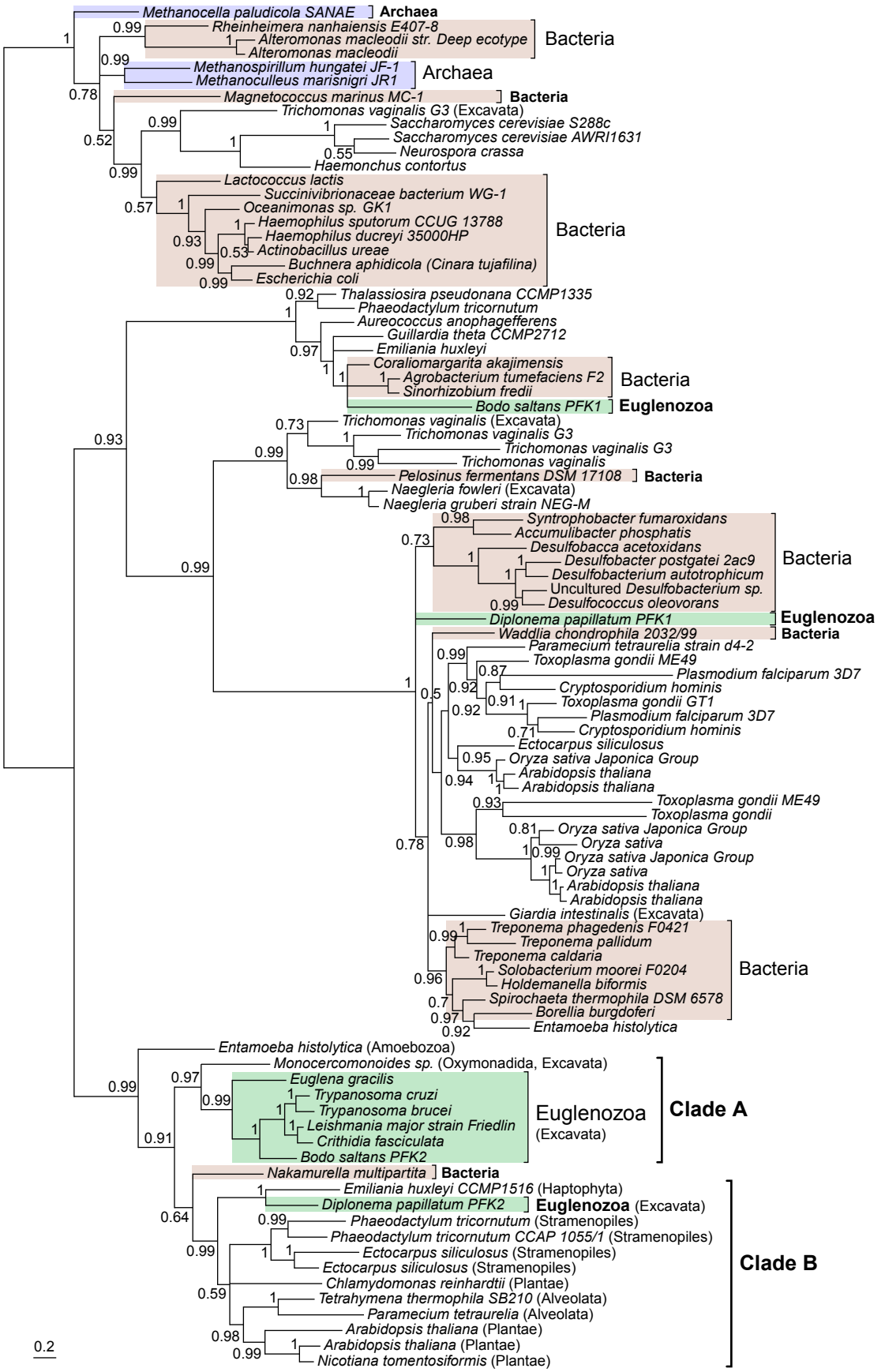
Methanocella paludicola SANAE
Archaea
Rheinheimera nanhaiensis E407-8
Alteromonas macleodii str. Deep ecotype
Alteromonas macleodii
Bacteria
Methanospirillum hungatei JF-1
Methanoculleus marisnigri JR1
Archaea
Magnetococcus marinus MC-1
Bacteria
Trichomonas vaginalis G3 (Excavata)
Saccharomyces cerevisiae S288c
Saccharomyces cerevisiae AWRI1631
Neurospora crassa
Haemonchus contortus
Lactococcus lactis
Succinivibrionaceae bacterium WG-1
Oceanimonas sp. GK1
Haemophilus sputorum CCUG 13788
Haemophilus ducreyi 35000HP
Actinobacillus ureae
Buchnera aphidicola (Cinara tujafilina)
Escherichia coli
Bacteria
Thalassiosira pseudonana CCMP1335
Phaeodactylum tricornutum
Aureococcus anophagefferens
Guillardia theta CCMP2712
Emiliania huxleyi
Coraliomargarita akajimensis
Agrobacterium tumefaciens F2
Sinorhizobium fredii
Bacteria
Bodo saltans PFK1
Euglenozoa
Trichomonas vaginalis (Excavata)
Trichomonas vaginalis G3
Trichomonas vaginalis G3
Trichomonas vaginalis
Pelosinus fermentans DSM 17108
Bacteria
Naegleria fowleri (Excavata)
Naegleria gruberi strain NEG-M
Syntrophobacter fumaroxidans
Accumulibacter phosphatis
Desulfobacca acetoxidans
Desulfobacter postgatei 2ac9
Desulfobacterium autotrophicum
Uncultured Desulfobacterium sp.
Desulfococcus oleovorans
Bacteria
Diplonema papillatum PFK1
Euglenozoa
Waddlia chondrophila 2032/99
Bacteria
Paramecium tetraurelia strain d4-2
Toxoplasma gondii ME49
Plasmodium falciparum 3D7
Cryptosporidium hominis
Toxoplasma gondii GT1
Plasmodium falciparum 3D7
Cryptosporidium hominis
Ectocarpus siliculosus
Oryza sativa Japonica Group
Arabidopsis thaliana
Arabidopsis thaliana
Toxoplasma gondii ME49
Toxoplasma gondii
Oryza sativa Japonica Group
Oryza sativa
Oryza sativa Japonica Group
Oryza sativa
Arabidopsis thaliana
Arabidopsis thaliana
Giardia intestinalis (Excavata)
Treponema phagedenis F0421
Treponema pallidum
Treponema caldaria
Solobacterium moorei F0204
Holdemanella biformis
Spirochaeta thermophila DSM 6578
Borellia burgdoferi
Entamoeba histolytica
Bacteria
Entamoeba histolytica (Amoebozoa)
Monocercomonoides sp. (Oxymonadida, Excavata)
Euglena gracilis
Trypanosoma cruzi
Trypanosoma brucei
Leishmania major strain Friedlin
Crithidia fasciculata
Bodo saltans PFK2
Euglenozoa
(Excavata)
Clade A
Nakamurella multipartita
Bacteria
Emiliania huxleyi CCMP1516 (Haptophyta)
Diplonema papillatum PFK2
Euglenozoa (Excavata)
Phaeodactylum tricornutum (Stramenopiles)
Phaeodactylum tricornutum CCAP 1055/1 (Stramenopiles)
Ectocarpus siliculosus (Stramenopiles)
Ectocarpus siliculosus (Stramenopiles)
Chlamydomonas reinhardtii (Plantae)
Tetrahymena thermophila SB210 (Alveolata)
Paramecium tetraurelia (Alveolata)
Arabidopsis thaliana (Plantae)
Arabidopsis thaliana (Plantae)
Nicotiana tomentosiformis (Plantae)
Clade B
0.2

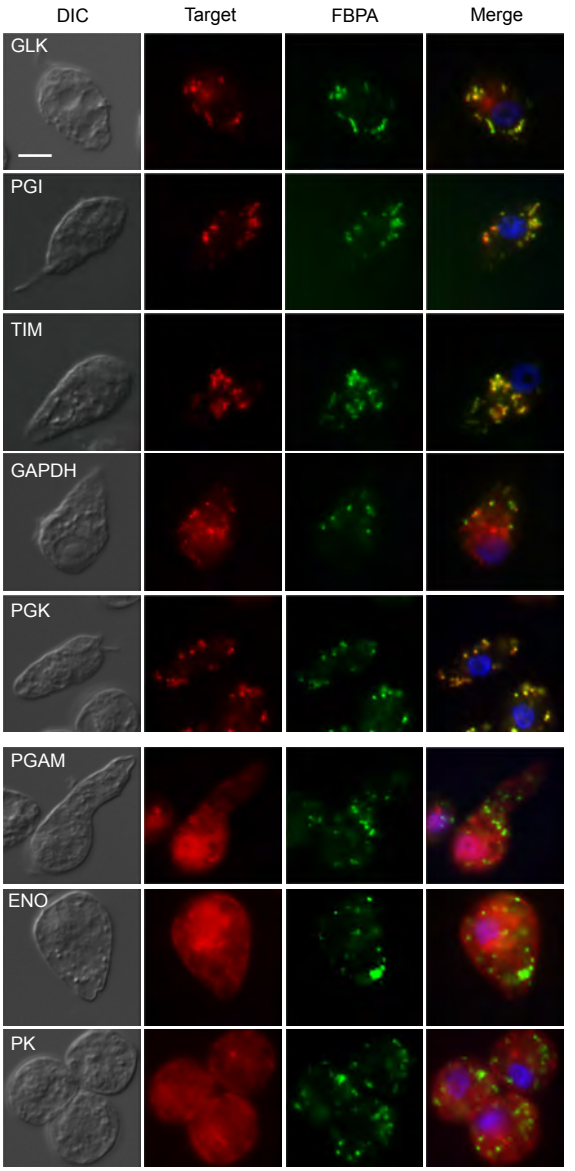
DIC
Target
FBPA
Merge
GLK
PGI
TIM
GAPDH
PGK
PGAM
ENO
PK

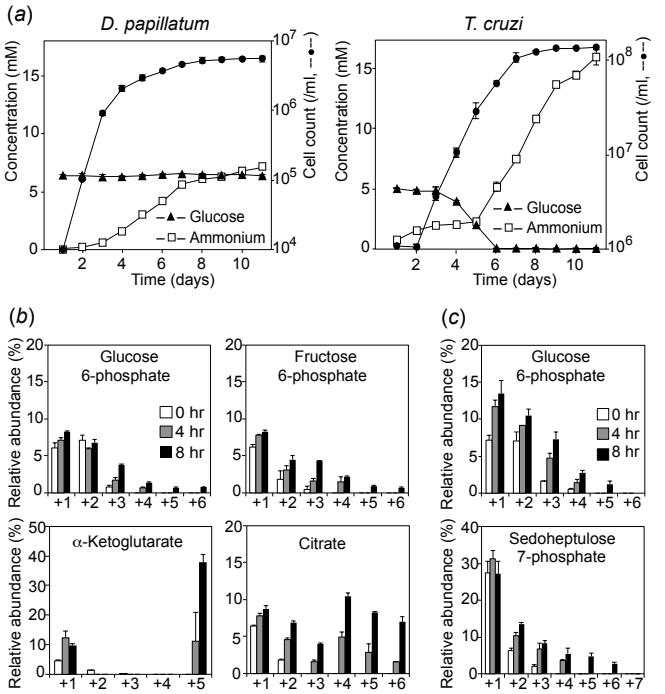
(a)
D. papillatum
T. cruzi
Concentration (mM)
Cell count (/ml, --●--)
Glucose
Ammonium
Time (days)
(b)
(c)
Relative abundance (%)
Glucose 6-phosphate
Fructose 6-phosphate
0 hr
4 hr
8 hr
α-Ketoglutarate
Citrate
Sedoheptulose 7-phosphate

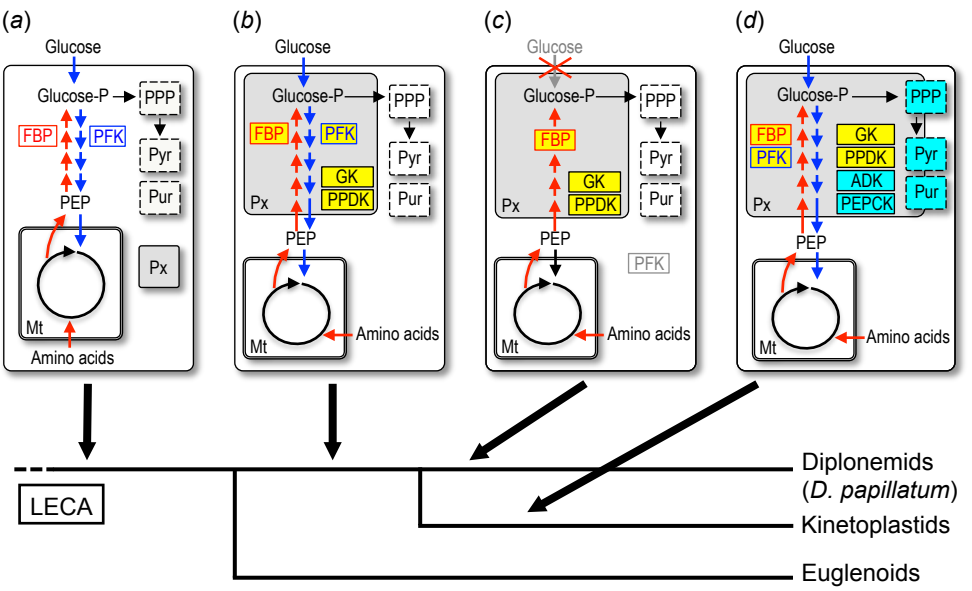
(a)
(b)
(c)
(d)
Glucose
Glucose-P
PPP
FBP
PFK
Pyr
Pur
PEP
Px
Mt
Amino acids
GK
PPDK
ADK
PEPCK
LECA
Diplonemids
(D. papillatum)
Kinetoplastids
Euglenoids

Differential remodelling of peroxisome function underpins the environmental and metabolic adaptability of diplonemids and kinetoplastids

Jorge Morales, Muneaki Hashimoto, Tom A. Williams, Hiroko Hirawake-Mogi, Takashi Makiuchi, Akiko Tsubouchi, Naoko Kaga, Hikari Taka, Tsutomu Fujimura, Masato Koike, Toshihiro Mita, Frédéric Bringaud, Juan L. Concepción, Tetsuo Hashimoto, T. Martin Embley and Takeshi Nara

Supplementary material

Supplementary materials and methods

(a) Enzyme activity

Cells of the mid-log phase were collected, washed twice with 10% (v/v) mannitol and resuspended in 50 mM Tris-HCl/2 mM EDTA pH 7 with protease inhibitor cocktail (Complete, Mini, Roche Diagnostics K.K., Tokyo, Japan). Cells were disrupted by sonication, centrifuged at 26,000 x *g* for 20 minutes, and the supernatant was used to measure the enzymatic activity described as follows; hexokinase and glucokinase [1], phosphoglucose isomerase [2], phosphofructokinase [3], fructose-1,6-biphosphate aldolase [4], GAPDH [5], triose-phosphate isomerase [6], phosphoglycerate kinase [7], phosphoglycerate mutase [8], enolase [9], pyruvate kinase [10], and fructose-1,6-biphosphatase [11].

(b) Antibodies

The mouse antiserum to *D. papillatum* FBPA was produced as described [12]. To obtain antisera to glycolytic enzymes, the cDNA clones of interest were obtained by PCR, cloned in pET151/D-TOPO vector, and expressed in BL21(DE3)Star cells (Life Technologies Japan Inc., Tokyo, Japan). The recombinant proteins were purified using His•Bind® Resin (Merck KGaA, Darmstadt, Germany) and used for raising antisera in rabbits or mice. Immunization of animals and collection of antisera were in part carried out by Medical & Biological Laboratories Co., Ltd., Nagoya, Japan. All animal experiments were carried out in accordance with the fundamental guidelines for animal experiments under the jurisdiction of the Ministry of Education, Culture, Sports, Science and Technology (Notice No. 71, 2006), and approved by the Committee for Animal Experimentation of Juntendo University with the Approval No. 270081.

(c) Western blots

20 μg of protein from the cell supernatant were separated onto a SuperSep® Ace 10-20 % gel (Wako Pure Chemical Industries, Ltd., Osaka, Japan) and transferred to a polyvinylidene fluoride membrane under semi-dry conditions at 20 V for 30 minutes. After blocking with 5% fetal bovine serum (FBS) in phosphate-buffered saline containing 0.25 % tween20 (PBST), the membranes were incubated overnight at 4°C with the antisera to each glycolytic enzyme in 1% FBS/PBST, washed with PBST, and incubated with HRP-conjugated secondary antibody (Jackson ImmunoResearch Laboratories Inc., PA), followed by chemiluminescent development. The reaction was visualized using ImageQuant LAS-4000 min (GE Healthcare Japan Inc., Tokyo, Japan).

(d) Electron microscopy

Cells of the late-log phase were harvested, washed twice in artificial marine water, and fixed as described [13]. Ultrathin sections were stained with lead citrate and uranyl acetate and examined with a transmission electron microscope at 75 kV (Hitachi H-7100, Hitachi High-Technologies Co. Ltd., Tokyo, Japan). For immunoelectron microscopy, cells were fixed using 4% paraformaldehyde and 1% glutaraldehyde in PBS at 4ºC for 2 hrs, dehydrated with ethanol, and embedded in LRWhite at -20ºC for 4 days under UV-light. Ultrathin sections were incubated with 50 mM NH_4Cl in PBS for 2 hours, blocked with 3% BSA in PBS/0.025 % tween20 for 1 hr, and incubated with antisera to *D. papillatum* FBPA [12] for 1 hr. Cells were then incubated with gold-labeled anti-mouse antibody (10 nm particle, Sigma-Aldrich Co. LLC., MO), counterstained with uranyl acetate, and observed using Hitachi H-7100.

(e) Metabolic labeling

The mid-log phase of cells were starved in artificial seawater for 2 hrs and then incubated with 6 mM $^{13}C_6$ D-glucose or 6 mM $^{13}C_5$ L-glutamine (Sigma-Aldrich) in artificial seawater for 0, 4, and 8 hrs or with 30 mM $^{13}C_6$ D-glucose in normal culture medium for 72 hrs without starvation. Cells in the mid-log phase of growth were starved in artificial seawater for 2 hrs and then incubated with 6 mM $^{13}C_6$ D-glucose or 6 mM $^{13}C_5$ L-glutamine (Sigma-Aldrich) in artificial seawater for 0, 4, and 8 hrs or with 30 mM $^{13}C_6$ D-glucose in normal culture medium for 72 hrs without starvation. Cells were then washed twice with 10% w/v mannitol and treated with methanol by vortexing for 1 min. After removing the debris by centrifugation, the supernatant was extracted with 1:0.4 of chloroform and milli-Q water by vortexing for 1 min. The aqueous phase was filtered through an Ultrafree MC PHLCC HMT filter (Merck KGaA, Darmstadt, Germany) having a cut-off of 5 kDa at 9,400 x *g* for 2 hrs to remove proteins. The eluate

containing the metabolites was evaporated and dissolved in 0.05 ml of Milli-Q water. CE-Q-TOFMS analysis was performed using an Agilent CE system combined with a Q-TOFMS (Agilent Technologies, Palo Alto, CA, USA) as described [14-16]. The data obtained by CE-Q-TOFMS analysis were preprocessed using MassHunter workstation software Qualitative Analysis Version B.06.00. Each metabolite was identified and quantified based on the peak information including m/z, migration time, and peak area. The quantified data were then evaluated for statistical significance by a Wilcoxon signed-rank test. Alternatively, liquid chromatography-coupled mass spectrometry (LC-MS) was performed on a TSQ Quantum Ultra AM with the analysis software Xcalibur 2.0.6 software (Thermo Fisher Scientific, San Jose, CA) coupled to a Gilson-HPLC system and a Gilson 234 autosampler (Gilson Inc., WI) as described [17].

(f) Metabolome analysis

Metabolome measurements were carried by Human Metabolome Technology Inc., Tsuruoka, Japan. Briefly, cells were collected in mid-log phase, washed twice with 10% mannitol, and resuspended in methanol containing internal standards (H3304-1002, Human Metabolome Technologies, Inc., Tsuruoka, Japan) followed by ultrasonication, to inactivate enzymes. The metabolites were further extracted and finally dissolved in 50 μL of Milli-Q water for CE-MS analysis.

References

1 Fujii S & Beutler E. 1985 High glucose concentrations partially release hexokinase from inhibition by glucose 6-phosphate. *Proc. Natl. Acad. Sci. USA* **82**, 1552-1554.

2 Misset O & Opperdoes FR. 1984 Simultaneous purification of hexokinase, class-I fructose-bisphosphate aldolase, triosephosphate isomerase and phosphoglycerate kinase from *Trypanosoma brucei*. *Eur. J. Biochem.* **144**, 475-483.

3 Sooranna SR & Saggerson ED. 1982 Rapid modulation of adipocyte phosphofructokinase activity by noradrenaline and insulin. *Biochem. J.* **202**, 753-758.

4 Galkin A, Kulakova L, Melamud E, Li L, Wu C, Mariano P, Dunaway-Mariano D, Nash TE & Herzberg O. 2007 Characterization, kinetics, and crystal structures of fructose-1,6-bisphosphate aldolase from the human parasite, *Giardia lamblia*. *J. Biol. Chem.* **282**, 4859-4867.

5 Molina y Vedia L, McDonald B, Reep B, Brüne B, Di Silvio M, Billiar TR & Lapetina EG. 1992 Nitric oxide-induced S-nitrosylation of glyceraldehyde-3-phosphate dehydrogenase inhibits enzymatic activity and increases endogenous ADP-ribosylation. *J. Biol. Chem.* **267**, 24929-24932.

6 Opperdoes FR & Borst P. 1977 Localization of nine glycolytic enzymes in a microbody-like organelle in *Trypanosoma brucei*: the glycosome. *FEBS Lett.* **80**, 360-364.

7 Yu JS & Noll KM. 1995 The hyperthermophilic bacterium *Thermotoga neapolitana* possesses two isozymes of the 3-phosphoglycerate kinase/triosephosphate isomerase fusion protein. *FEMS Microbiol. Lett.* **131**, 307-312.

8 Chevalier N, Rigden DJ, Van Roy J, Opperdoes FR & Michels PA. 2000 *Trypanosoma brucei* contains a 2,3-bisphosphoglycerate independent phosphoglycerate mutase. *Eur. J. Biochem.* **267**, 1464-1472.

9 Hannaert V, Albert MA, Rigden DJ, da Silva Giotto MT, Thiemann O, Garratt RC, Van Roy J, Opperdoes FR & Michels PA. 2003 Kinetic characterization, structure modelling

studies and crystallization of *Trypanosoma brucei* enolase. *Eur. J. Biochem.* **270**, 3205-3213.

10 Callens M, Kuntz DA & Opperdoes FR. 1991 Characterization of pyruvate kinase of *Trypanosoma brucei* and its role in the regulation of carbohydrate metabolism. *Mol. Biochem. Parasitol.* **47**, 19-29.

11 Misek DE & Saltiel AR. 1992 An inositol phosphate glycan derived from a *Trypanosoma brucei* glycosyl-phosphatidylinositol mimics some of the metabolic actions of insulin. *J. Biol. Chem.* **267**, 16266-16273.

12 Makiuchi T, Annoura T, Hashimoto M, Hashimoto T, Aoki T & Nara T. 2011 Compartmentalization of a glycolytic enzyme in *Diplonema*, a non-kinetoplastid euglenozoan. *Protist* **162**, 482-489. (doi:10.1016/j.protis.2010.11.003).

13 Marande W, Lukeš J & Burger G. 2005 Unique mitochondrial genome structure in diplonemids, the sister group of kinetoplastids. *Eukaryot. Cell* **4**, 1137-1146.

14 Kami K, Fujimori T, Sato H, Sato M, Yamamoto H, Ohashi Y, Sugiyama N, Ishihama Y, Onozuka H, Ochiai A, et al. 2013 Metabolomic profiling of lung and prostate tumor tissues by capillary electrophoresis time-of-flight mass spectrometry. *Metabolomics* **9**, 444-453. (doi:10.1007/s11306-012-0452-2).

15 Ohashi Y, Hirayama A, Ishikawa T, Nakamura S, Shimizu K, Ueno Y, Tomita M & Soga T. 2008 Depiction of metabolome changes in histidine-starved *Escherichia coli* by CE-TOFMS. *Mol. Biosyst.* **4**, 135-147. (doi:10.1039/b714176a).

16 Ooga T, Sato H, Nagashima A, Sasaki K, Tomita M, Soga T & Ohashi Y. 2011 Metabolomic anatomy of an animal model revealing homeostatic imbalances in dyslipidaemia. *Mol. Biosyst.* **7**, 1217-1223. (doi:10.1039/c0mb00141d).

17 Olszewski KL, Mather MW, Morrisey JM, Garcia BA, Vaidya AB, Rabinowitz JD & Llinas M. 2010 Branched tricarboxylic acid metabolism in *Plasmodium falciparum*. *Nature* **466**, 774-778. (doi:10.1038/nature09301).

Table S1. Predicted PTS in non-glycolytic enzymes of *Diplonema papillatum*.

Enzyme	PTS*	
	D. papillatum	***T. brucei***
Gluconeogenesis		
Malate dehydrogenase (MDH), glycosomal	ND	PTS1
Phosphoenolpyruvate carboxykinase (PEPCK)	ND	PTS1
Pentose phosphate pathway		
6-phosphogluconolactonase	ND	PTS1
Ribokinase	ND	PTS1
Transketolase	ND	PTS1
Energy/redox metabolism		
Adenylate kinase	ND	PTS1
Glycerol 3-phosphate dehydrogenase	ND	PTS1
Glycerol kinase (GK)	PTS1	PTS1
Isocitrate dehydrogenase	ND	PTS1
NADH-dependent fumarate reductase	ND	PTS1
Pyruvate phosphate dikinase (PPDK)	PTS1	PTS1
Pyrimidine biosynthesis/purine salvage		
Adenine phosphoribosyltransferase	ND	PTS1
Guanylate kinase	ND	PTS1
Hypoxanthine-guanine phosphoribosyltransferase	ND	PTS1
Inosine-5'-monophosphate dehydrogenase	ND	PTS1
Orotate phosphoribosyltransferase (OPRT)	ND	PTS1†
Orotidine monophosphate decarboxylase (OMPDC)	ND	PTS1†

*PTS1 represents being double positive for both the C-terminal consensus tripeptides, (STAGCN)-(RKH)-(LIVMAFY), and a category of “targeted” or “twilight zone” using the PTS1 predictor (see materials and methods).
†Fused in OMPDC-OPRT.
ND; No PTS detected.

Table S2. Metabolites of carbon metabolism in *Diplonema papillatum*.

Metabolites (pmole/10^8 cells)	*T. cruzi*	*D. papillatum*[a]	*D. papillatum*[b]	*D. papillatum*[c]
Glycolysis				
Hexose phosphate group				
Glucose 6-phosphate	161	21,166	37,182	6,168
Glucose 1-phosphate	77	4,393	5,773	1,435
Fructose 6-phosphate	348	7,895	13,324	2,739
Fructose 1,6-bisphosphate	158	3,490	2,203	769
Triose phosphate group				
Dihydroxyacetone phosphate	129	11,779	5,944	2,600
Glyceraldehyde 3-phosphate	ND	186	ND	ND
3-Phosphoglyceric acid	1,707	4,080	4,442	1,003
2-Phosphoglyceric acid	267	638	777	189
Phosphoenolpyruvic acid	1,036	564	903	ND
Ratio of total hexose-P:triose-P	**744:3149 (1:4.2)**	**36944:17247 (2.1:1)**	**58482:12066 (4.8:1)**	**11111:3792 (2.9:1)**
TCA cycle				
Citric acid	330	1,705	894	401
cis-aconitic acid	ND	924	532	237
Isocitric acid	ND	70,382	53,107	21,083
α-ketoglutaric acid	ND	4,397	4,412	3,180
Succinic acid	35,203	108,395	113,315	22,092
Fumaric acid	126	6,454	2,204	1,492
Malic acid	535	22,612	15,545	9,739
Pentose phosphate pathway				
6-Phosphogluconic acid	21	73	ND	ND
Ribulose 5-phosphate	144	1,859	1,906	511
Ribose 5-phosphate	38	585	638	128
Sedoheptulose 7-phosphate	282	1,729	5,199	443
Erythrose 4-phosphate	ND	572	353	ND
Nucleotides				
ATP	8,578	6,944	9,481	1,247
ADP	8,010	19,800	19,395	6,637
AMP	8,028	50,665	23,739	14,455
cAMP	15	ND	ND	ND
GTP	2,264	1,228	2,116	607
GDP	2,196	4,572	4,143	2,223
GMP	1,208	6,643	3,884	3,248
UTP	4,974	1,984	2,259	290
UDP	5,083	4,847	4,626	1,502
UMP	5,571	11,936	5,445	2,657
CTP	583	139	400	ND
CDP	360	302	528	280
CMP	457	2,560	2,407	1,424

[a] ATCC® 1405 artificial seawater supplemented with 10 % v/v horse serum.
[b] ATCC® 1532 medium.
[c] ATCC® 1532 medium supplemented with 6 mM D-glucose.
ND, not detected.

Table S2. *Continued.*

Metabolites (pmole/10^8 cells)	*T. cruzi*	*D. papillatum*[a]	*D. papillatum*[b]	*D. papillatum*[c]
Others				
Pyruvic acid	126	1,372	2,351	1,820
Lactic acid	11,800	82,962	84,245	20,330
Amino acids				
β-Ala	147	1,191,232		
Glu	14,748	842,686		
Lys	20,288	453,660		
Pro	17,256	423,095		
Ala	212,561	367,248		
Gln	86	317,801		
Arg	11,335	217,878		
Gly	99,373	137,363		
Val	36,898	134,090		
His	200	109,362		
Ser	507	98,449		
Thr	338	85,611		
Leu	3,968	78,799		
Tyr	929	73,437		
Asn	1,700	53,480		
Asp	1,578	51,883		
Ile	15,529	35,984		
Phe	808	35,481		
Trp	290	15,796		
Met	244	12,534		
Cys	ND	569		

[a] ATCC® 1405 artificial seawater supplemented with 10 % v/v horse serum.
[b] ATCC® 1532 medium.
[c] ATCC® 1532 medium supplemented with 6 mM D-glucose.
ND, not detected.

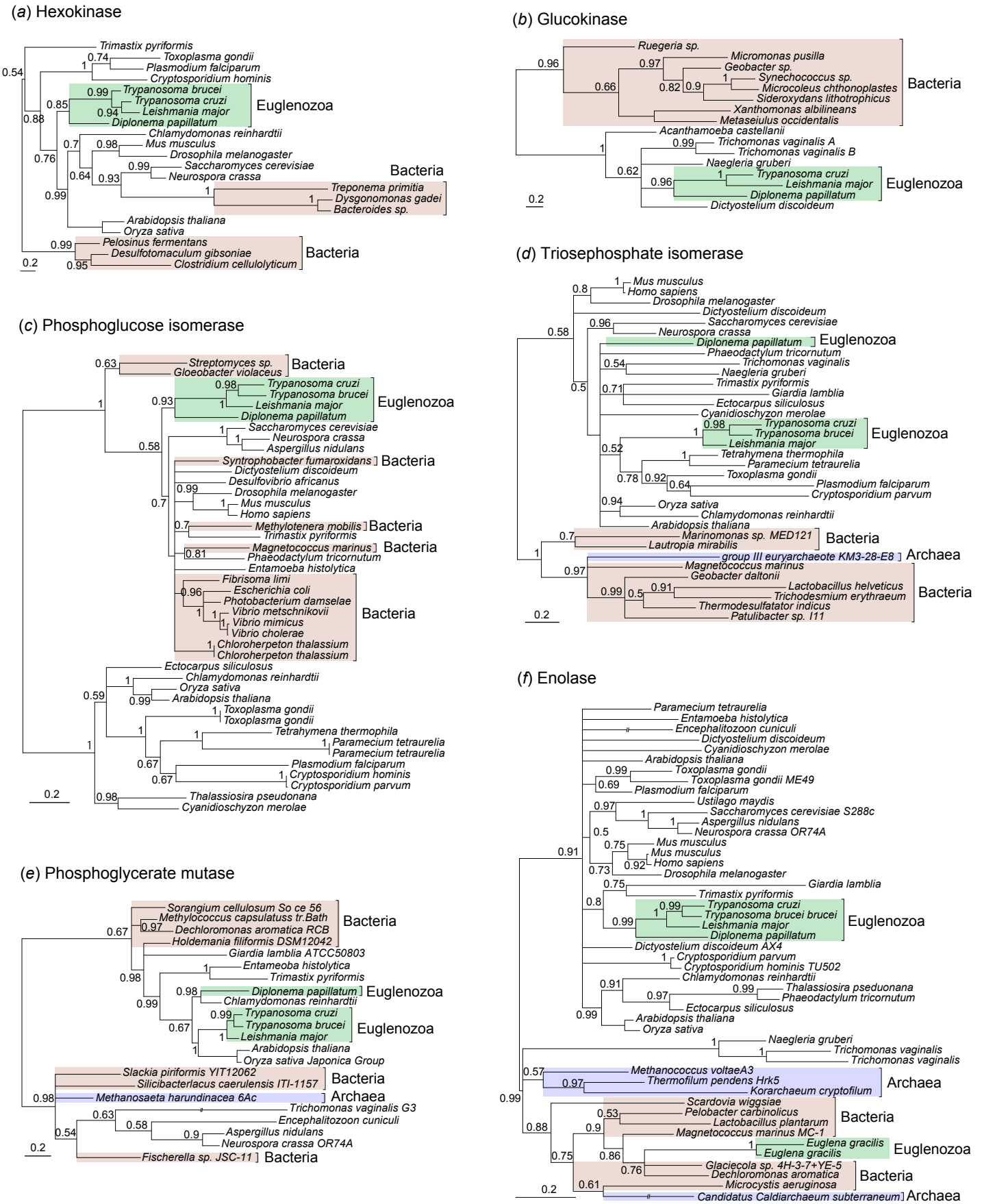

Figure S1. Consensus phylogenetic trees for glycolytic enzymes. (*a*) Hexokinase; (*b*) glucokinase; (*c*) phophoglucose isomerase; (*d*) triose phosphate isomerase; (*e*) phophoglycerate mutase; and (*f*) enolase. Euglenozoa, bacteria and archaea are labeled in green, brown, and gray, respectively. The detailed methods to reconstruct the phylogenetic trees are described in the materials and methods.

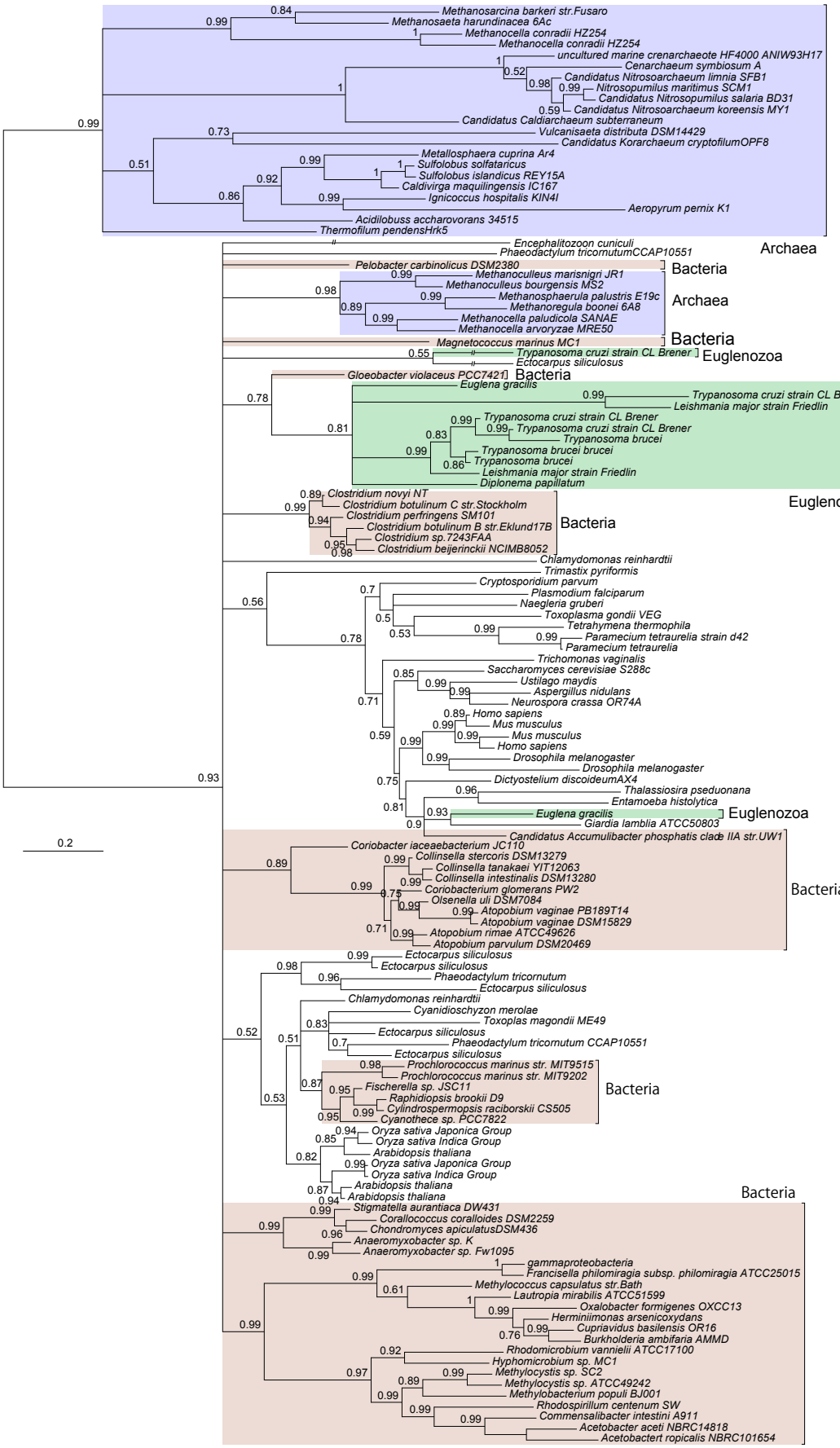

Figure S2. Consensus phylogenetic tree for phosphoglycerate kinase. The methods and labeling are as in figure S1.

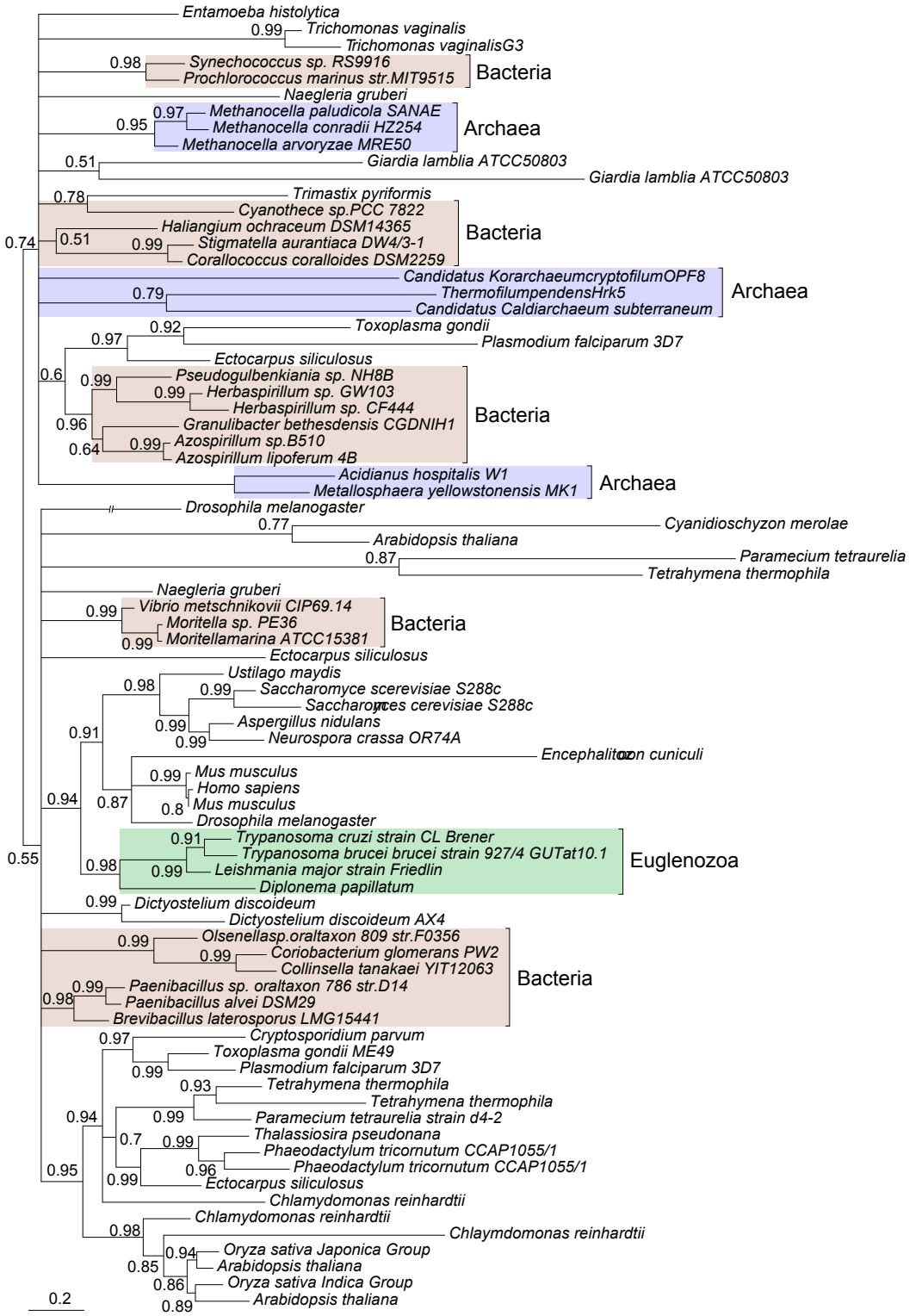

Figure S3. Consensus phylogenetic tree for pyruvate kinase. The methods and labeling are as in figure S1.

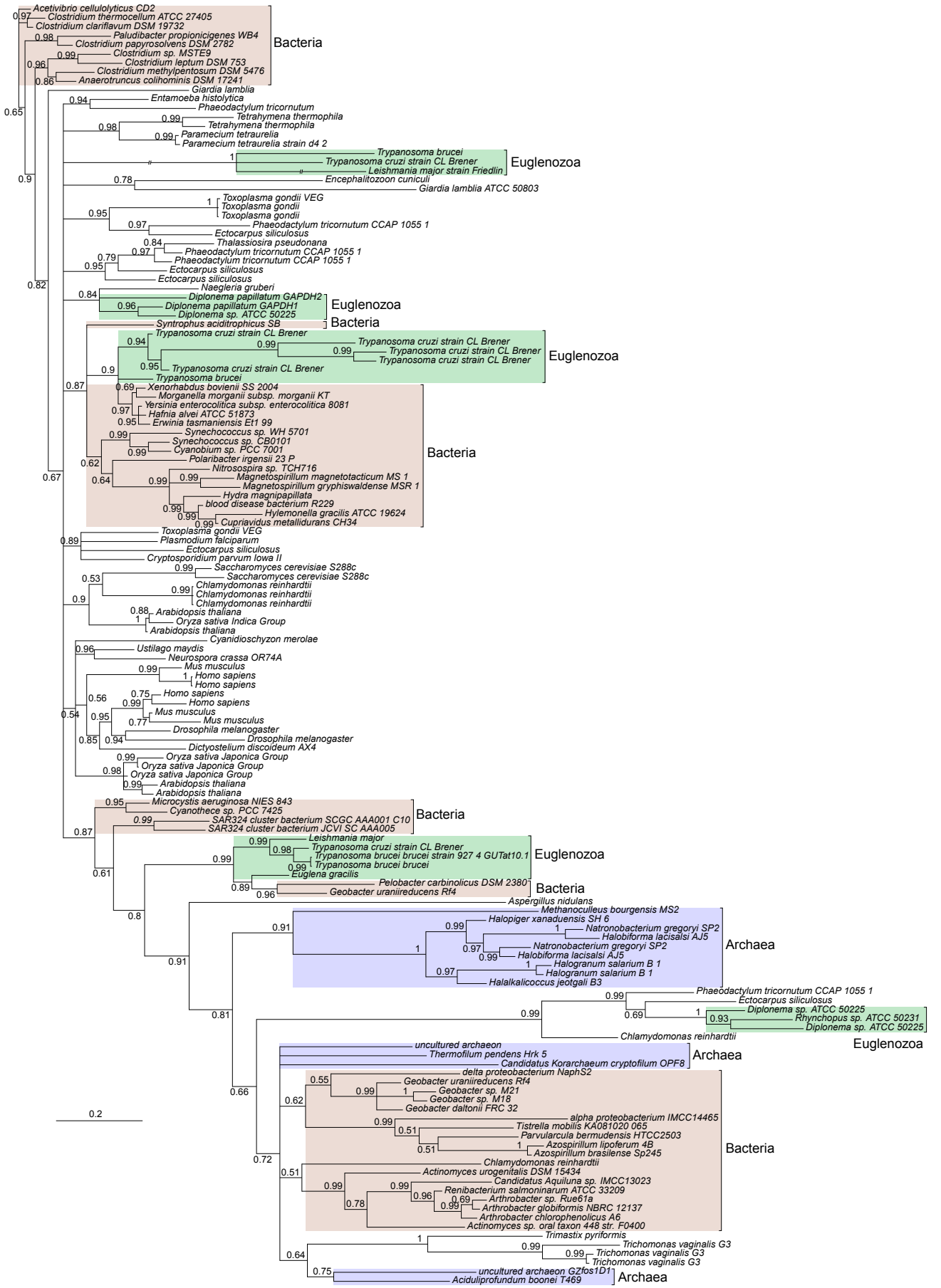

Figure S4. Consensus phylogenetic tree for glyceraldehyde-3-phosphate dehydrogenase. The methods and labeling are as in figure S1.

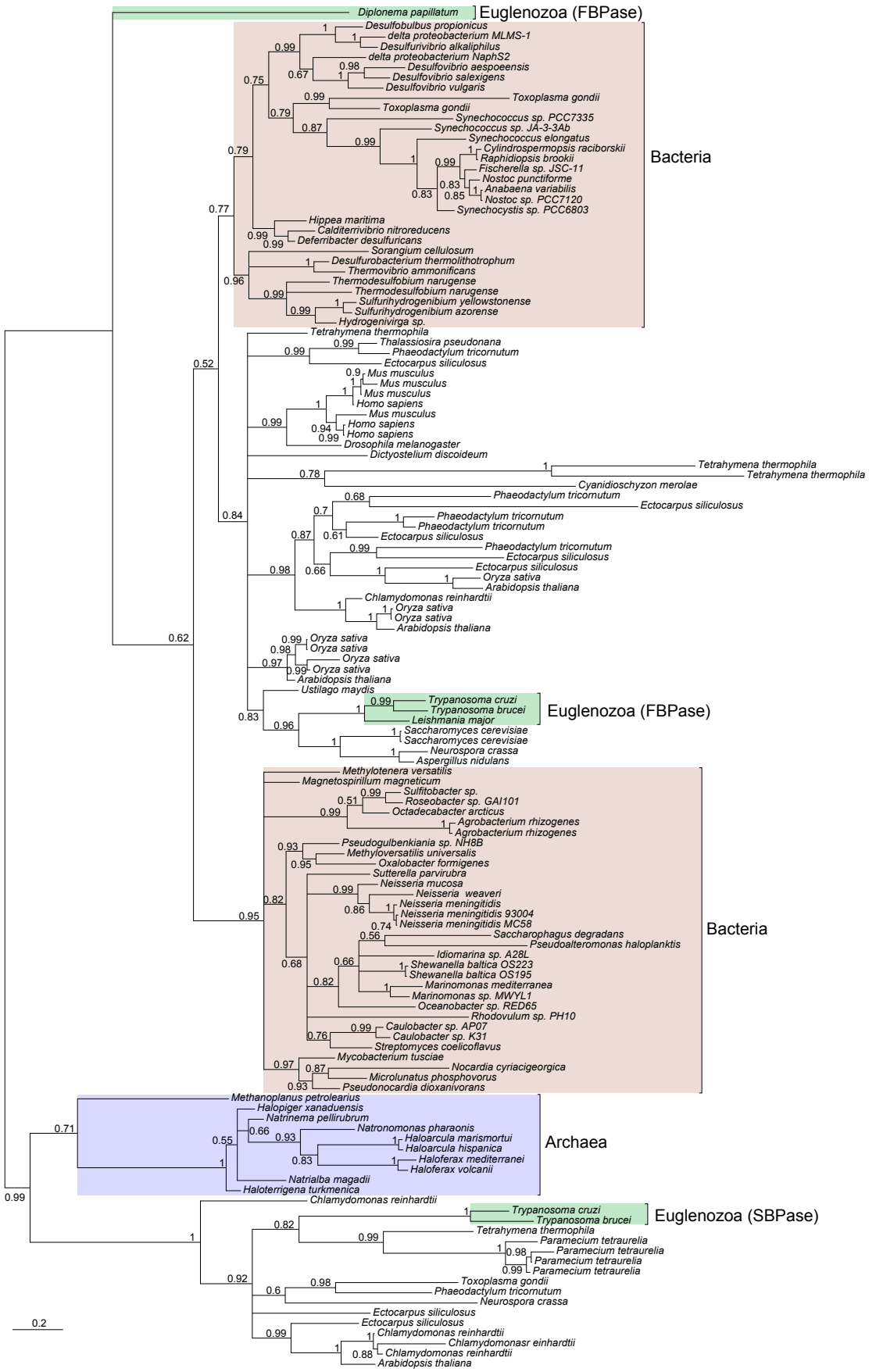

Figure S5. Consensus phylogenetic tree for fructose-1,6-bisphosphatase (FBPase). Sedoheptulose-1,7-bisphosphatase (SBPase) is an enzyme for pentose phosphate pathway. The methods and labeling are as in figure S1.

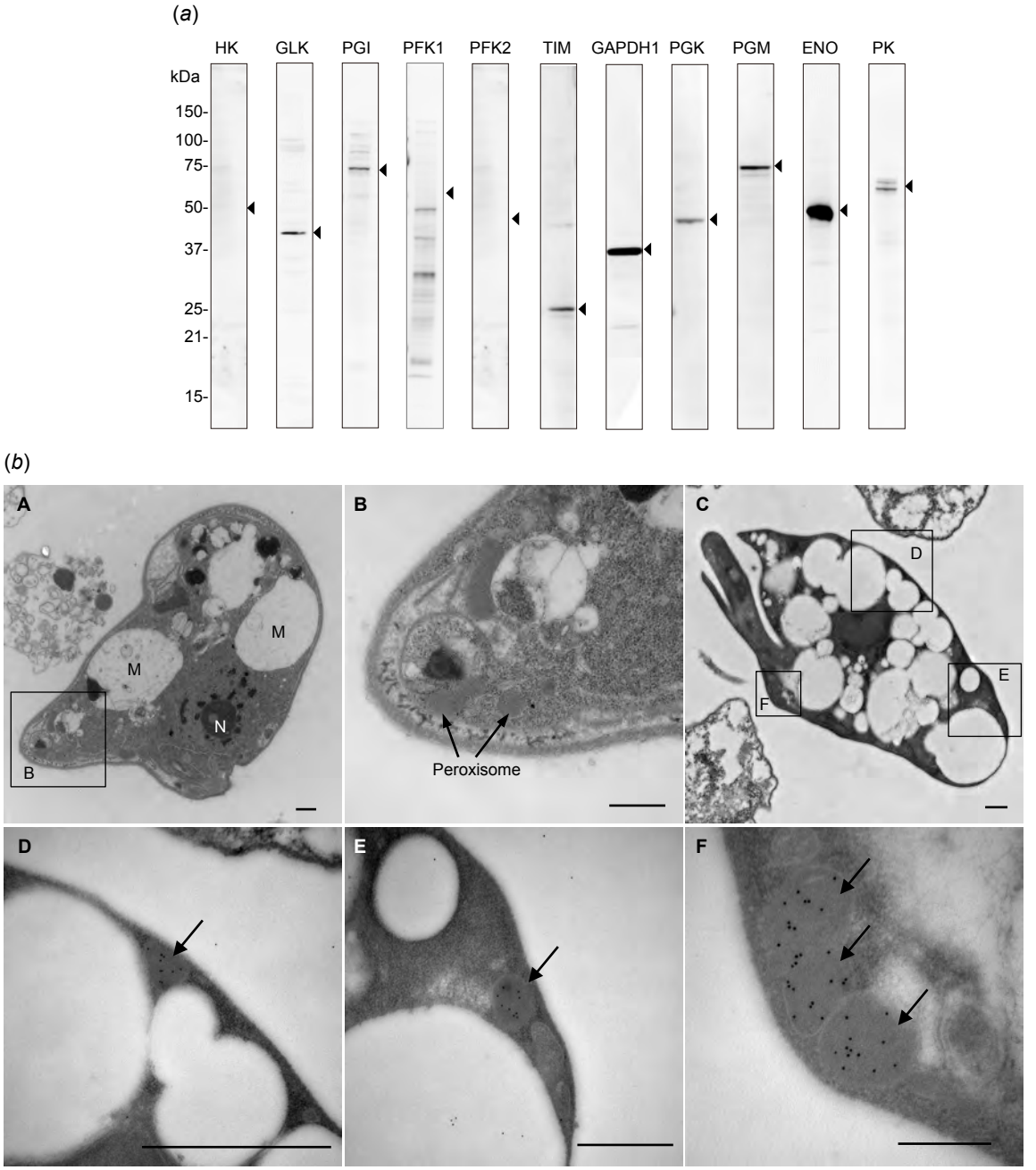

Figure S6. Expression of glycolytic enzymes in *D. papillatum*. (*a*) Western blot analysis of the *D. papillatum* extracts using antisera to the relevant enzymes. The expected size of each protein is shown by a triangle in each panel. (*b*) Ultrastructure of *D. papillatum*. Peroxisomes (arrow) are present as dense bodies surrounded by a single-membrane (B, a magnified image of the inset of A). C-F, Immunoelectron microscopic observations of FBPA within peroxisomes. Note that gold particles are specifically detected inside peroxisomes (arrow). (D, E, and F are magnified images of the insets of C). N; nucleus. M; mitochondrion, P; peroxisome. Scale bar = 0.5 μm.

(*a*) 6 mM $^{13}C_5$-L-glutamine

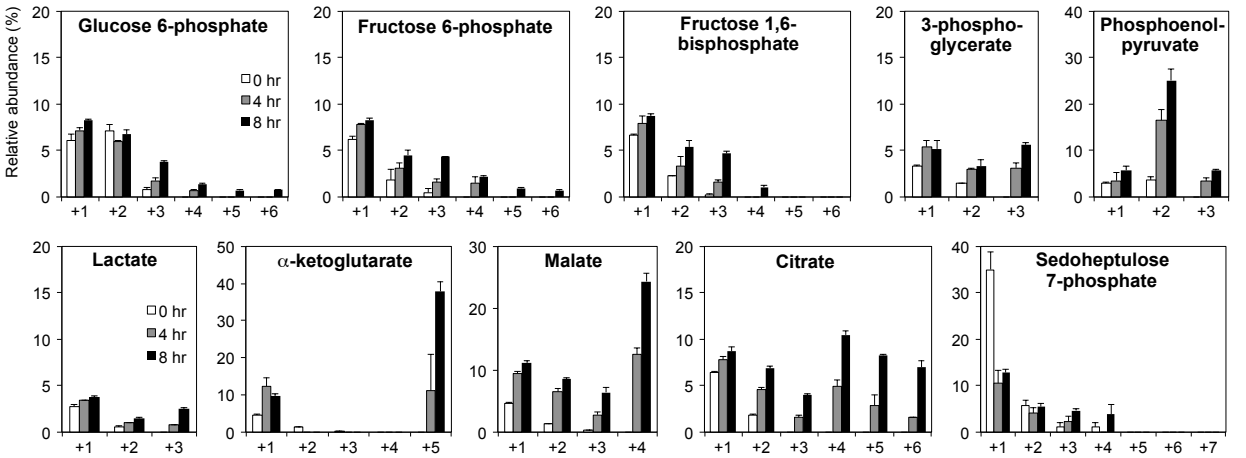

(*b*) 6 mM $^{13}C_6$-D-glucose

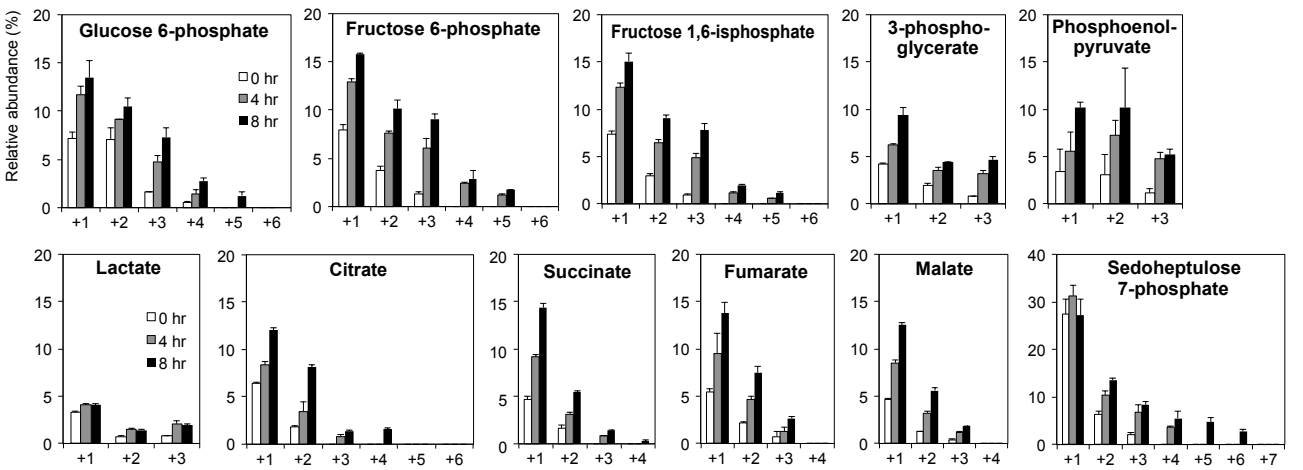

(*c*) 30 mM $^{13}C_6$-D-glucose

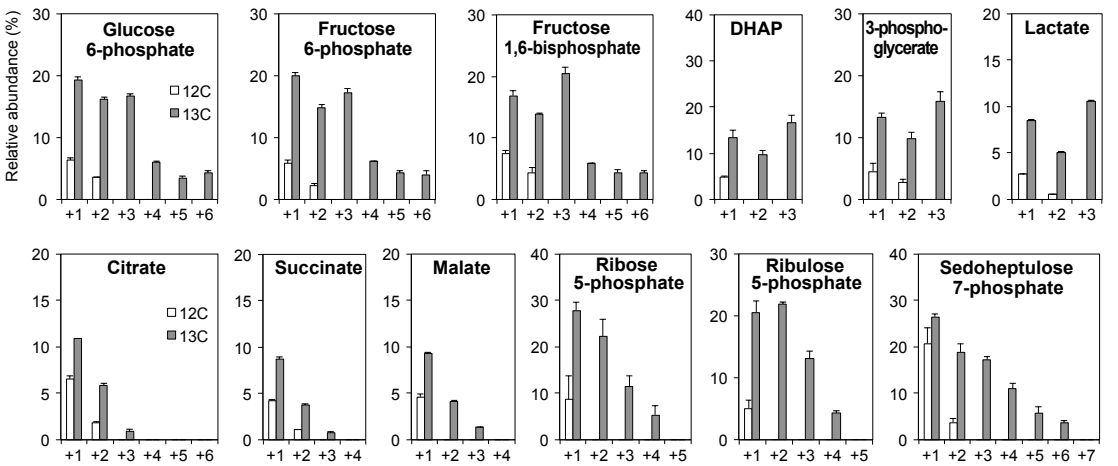

Figure S7. Metabolomic analysis of ^{13}C-labeled metabolites in *D. papillatum*. *D. papillatum* cells were incubated with 6 mM $^{13}C_5$-glutamine for 0, 4, and 8 hrs (*a*), 6 mM $^{13}C_6$-D-glucose for 0, 4, and 8 hrs (*b*), or 30 mM $^{13}C_6$-D-glucose for 72 hrs (*c*). The Y-axis indicates the relative abundance (%) of each isotopomer of the relevant metabolite. The X-axis represents the number of ^{13}C in the isotopomers. Data points and error bars represent the mean ± s.d. of three independent experiments.

Figure S8. Consensus phylogenetic tree for adenylate kinase. Note that *E. gracilis* enzyme and the glycosomal enzymes of kinetoplastids are nested independently within the bacterial clade (PP = 0.99), while *D. papillatum* and cytosolic kinetoplastid homologues cluster in the eukaryotic subtree (PP = 0.99). The methods and labeling are as in figure S1.

Figure S9. Consensus phylogenetic tree for inosine-5-monophosphate dehydrogenase. Note that glycosomal isoforms of kinetoplastids are nested within the bacterial clade, while *E. gracilis*, *D. papillatum* and cytosolic kinetoplastid homologues are monophyletic and cluster in the eukaryotic clade, consistent with the organismal tree (PP = 1). The methods and labeling are as in figure S1.

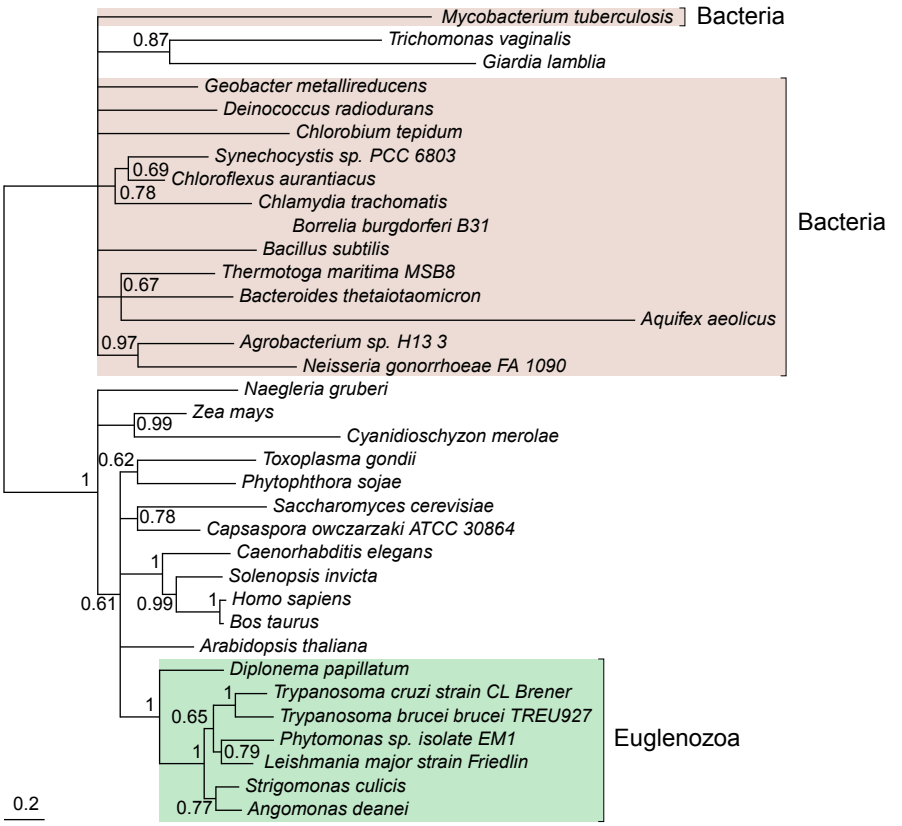

Figure S10. Consensus phylogenetic tree for transketolase. Note that the euglenozoan enzymes are monophyletic (PP = 1). The methods and labeling are as in figure S1.